



# Synthesis of mesoporous crosslinked polyaniline using SDS as a soft template for high-performance supercapacitors

Mingwei Shi<sup>1</sup> , Mengdi Bai<sup>1</sup> , and Baoming Li<sup>1,\*</sup> 

<sup>1</sup> College of Material Science and Engineering, Fuzhou University, Fuzhou 350108, People's Republic of China

**Received:** 14 January 2018

**Accepted:** 28 March 2018

**Published online:**  
4 April 2018

© Springer Science+Business Media, LLC, part of Springer Nature 2018

## ABSTRACT

Mesoporous crosslinked polyaniline (MCP) was prepared by chemically copolymerizing aniline and *p*-phenylenediamine with triphenylamine as cross-linker, using ammonium persulfate as an oxidant and sodium dodecylsulfate as a soft template. Disordered mesoporous structure of MCP was suggested by SEM observation, TEM observation and BET analysis. Nitrogen adsorption-desorption isotherm revealed that the specific surface area of MCP was up to 59.1 m<sup>2</sup>/g. In addition, MCP exhibited a high specific capacitance of 516 F/g at 2 A/g and a remarkable electrochemical cycling stability with the specific capacitance retention of 73.2% after 2000 cycles, which was better than polyaniline with a specific capacitance of 293 F/g at 2 A/g and the specific capacitance retention of 48.2% after 2000 cycles. The improved specific capacitance and electrochemical cycling stability of MCP were essentially attributed to the synergistic effects of special mesoporous crosslinked structure, high conductivity and large specific surface area.

## Introduction

In recent years, supercapacitors have attracted more and more attentions because of their high-power delivery within a very short time and a long cycling life, which could store large amounts of energy [1]. Supercapacitors could be divided into two types according to their charge-storage mechanisms [2], the one was electrical double-layer capacitor (EDLC), where the capacitance arose from the charge separation at an electrode/electrolyte interface, and the other was the redox supercapacitor, where the

capacitance came from Faradic reaction of the electrode materials. The electrode materials used for EDLC were mainly carbon materials [3], whose effective surface areas limited severely the specific capacitance of EDLC [4]. The electrode materials for redox supercapacitor included noble metal oxides [5] and electrically conducting polymers (ECPs) [6]. Compared with carbon materials, noble metal oxides exhibited high specific capacitance, for instance, the specific capacitance of RuO<sub>2</sub> could reach up to 982 F/g [7], but noble metal oxides were too expensive to commercialize. ECPs had advantages over noble

Address correspondence to E-mail: libaoming@fzu.edu.cn

metal oxides because of their low costs and simple synthetic methods, and had advantages over carbon materials due to their large specific capacitances and great redox reversibility [8]. Regrettably, as the electrode materials for supercapacitors, ECPs exhibited limited specific capacitance owing to their low specific surface areas and poor cycling stabilities as a result of volume change during the long charge–discharge process [9–11].

Till date, many attentions have been paid to the synthesis of high electroactive ECP composites by using porous carbons as supporting materials for supercapacitors, which have contributed to the improvement in cycling stability and the achievement of large specific surface area. For example, Li et al. [12] prepared a high-performance polyaniline (PANI) electrode by potentiostatic deposition of aniline on a hierarchically porous carbon monolith that was obtained by carbonization from the mesophase pitch. However, each component in the high electroactive ECP composites synthesized using porous carbons as supporting materials was prone to retain its own structure and the improvement in cycling stability and their large specific surface areas were not thanks to ECPs themselves, but mainly ascribed to the contributions of these supporting materials.

Crosslinked structure might be a candidate for improving the electrical and electrochemical properties of ECPs. Wang et al. [13] prepared crosslinked PANI (CPANI) via in situ chemical oxidative polymerization in the presence of *p*-phenylenediamine (PPDA) and triphenylamine (TPA), and discussed the application of CPANI as an electrode material for supercapacitors. However, it was found that CPANI only showed rod-like structure with low specific surface area, which was clearly unfavorable to the improvement in specific capacitance.

The soft template synthesis, also named self-assembly, was a process in which a disordered pre-polymerization system formed an organized nanostructure after polymerization as a consequence of local interactions among the monomers and the surfactants themselves without external direction [14]. The soft template synthesis owned the advantages of low cost and high yield, which was suitable for the production in large quantities in one pot [14]. Mai et al. [15, 16] prepared 2D mesoporous N-doped carbon/reduced graphene oxide nanosheets (mNC/rGO) and PANI/MoS<sub>2</sub> nanocomposites by using polystyrene-block-poly (ethylene oxide) (PS-*b*-PEO)

block copolymer as the soft template. The results showed that the mNC/rGO nanosheets had an average pore size of 19 nm and a high specific surface of 812 m<sup>2</sup>/g, and the PANI/MoS<sub>2</sub> nanocomposites with a high specific capacitance of 375 F/g at 1 A/g exhibited a good electrochemical cycling stability owing to its porous structure and MoS<sub>2</sub> nanosheets as support material. Guo et al. [17–19] utilized sodium dodecylsulfate (SDS) and HCl solution to control the morphology of PANI and obtain PANI in the forms of granules, nanofibers, nanosheets, rectangular sub-microtubes, porous structures and fanlike/flowerlike aggregates by regulating the concentrations of SDS and HCl. Xin et al. [20] synthesized N-doped mesoporous carbons (N-MCs) via the oxypolymerization of aniline with an F127 template, sintering at 850 °C in N<sub>2</sub> atmosphere, and activation in a KOH solution. The specific capacitances of N-MCs were 318 F/g at 0.2 A/g, and the cycle life of N-MCs at different current densities was above 96% after 5000 cycles of charging and discharging.

Herein, we synthesized mesoporous crosslinked polyaniline (MCP) with pore diameter of 5–35 nm by chemically copolymerizing aniline and PPDA with TPA as crosslinker, using SDS as a soft template and ammonium persulfate (APS) as an oxidant. SDS as an emulsifier was conducive to the uniform dispersion of TPA in acid solution, which allowed a high extent of copolymerization. The framework of MCP was composed of CPANI moieties and played an important role in the stability of mesoporous structure, which was beneficial to the improvements of specific capacitance and its electrochemical cycling stability.

## Experimental procedure

### Materials

Aniline was obtained from Sinopharm Chemical Reagent Co., Ltd. (Shanghai, China) and distilled under reduced pressure before use. PPDA, TPA, APS, sulfuric acid (H<sub>2</sub>SO<sub>4</sub>), ammonium hydroxide (NH<sub>3</sub>·H<sub>2</sub>O), *N*-methylpyrrolidone (NMP) and *N,N*-dimethylformamide (DMF) were all obtained from Sinopharm Chemical Reagent Co., Ltd. (Shanghai, China) and used as received. Deionized (DI) water was used throughout the experiment.

## Synthesis of CPANI and PANI

CPANI was synthesized by chemical oxidative polymerization, and the feeding molar ratio of SDS to aniline was varied as 1:1, 3:1, 5:1, 7:1 and 10:1. First, a certain amount of SDS was added to 100 mL of 0.1 mol/L  $\text{H}_2\text{SO}_4$  in a 250-mL round-bottom flask and stirred for 30 min. Next, a mixture of freshly distilled aniline (0.005 mol), TPA ( $5 \times 10^{-5}$  mol) and PPDA ( $1 \times 10^{-4}$  mol) was added into the above solution and stirred for 30 min. Then, 0.005 mol APS in 20 mL of 0.1 mol/L  $\text{H}_2\text{SO}_4$  was added drop by drop into the above solution and the solution continued to be stirred at 25 °C for 12 h. Finally, 100 mL methanol was added into the above reaction mixture and CPANI powder was filtered and washed repeatedly with methanol, ethanol and DI water to remove residual chemical agents, oligomers and SDS until the filtrate was colorless. For comparison, PANI without SDS, PPDA and TPA was synthesized under the same reaction conditions.

## De-doping and re-doping of MCP

First, the obtained CPANI powder was added into 100 mL of 1 mol/L  $\text{NH}_3\cdot\text{H}_2\text{O}$  and stirred at 25 °C for 8 h. Next, the precipitates were collected and washed repeatedly with ethanol and DI water to remove SDS and  $\text{NH}_3\cdot\text{H}_2\text{O}$  until the pH value of filtrate was 7 in order to obtain the de-doped MCP. Then, the de-doped MCP was added into 100 mL of 1 mol/L  $\text{H}_2\text{SO}_4$  and stirred at 25 °C for 8 h. Finally,  $\text{H}_2\text{SO}_4$  re-doped MCP was obtained after the precipitates were collected and washed repeatedly with ethanol and DI water until the filtrate was colorless. For the convenience of discussion, the resulting  $\text{H}_2\text{SO}_4$  re-doped MCP samples were designated as MCP-1, MCP-2, MCP-3, MCP-4 and MCP-5 according to the feeding molar ratio of SDS to aniline.

## Measurements

Fourier transform infrared (FT-IR) spectrum and UV-Vis absorption spectrum were recorded by Nicolet 5700 Fourier transform infrared spectrometer and Hitachi U-2001 UV-Visible spectrometer, respectively. SEM observation was taken using a Zeiss SUPRA 55 scanning electron microscopy at an accelerating voltage of 3 kV. TEM observation was taken using a FEI Tecnai G2 F20 S-TWIN

transmission electron microscopy at an accelerating voltage of 80 kV. XRD measurement was conducted on X'Pert Pro MPD using  $\text{Cu K}\alpha_1$  irradiation at a rate of 5°/min from 5° to 40°. TGA was performed by a Seiko SSC5200 thermal analyzer at a heating rate of 10 °C/min under flowing  $\text{N}_2$  gas. The specific surface area was measured at 77 K by nitrogen adsorption-desorption isotherm with a 3 Flex surface area analyzer and calculated with the Brunauer-Emmett-Teller (BET) method. The conductivity was recorded using a RTS-2 four-point probe conductivity tester at 25 °C.

All the electrochemical experiments were carried out in a three electrode system with a working electrode, a platinum counter electrode and a standard calomel reference electrode (SCE). The working electrode was fabricated with a mixture containing about 4 mg active material, 0.75 mg carbon black and 0.25 mg polyvinylidene uoride (PVDF) to prepare a homogeneous mixture in NMP. Cyclic voltammetry (CV), galvanostatic charge-discharge (GCD) and electrochemical impedance spectroscopy (EIS) were performed on a CHI660D electrochemical workstation in a 1 mol/L  $\text{H}_2\text{SO}_4$  aqueous solution. The potential range for CV and GCD tests was  $-0.2$  to 0.8 V. EIS test was carried out in the frequency range of 100 kHz to 0.01 Hz with an AC perturbation of 5 mV.

## Results and discussion

### Spectral studies

FT-IR spectra of SDS, PANI and MCP-3 are shown in Fig. 1. It was found that the peaks attributed to the C = C stretching vibrations of quinoid ring and benzenoid ring in FT-IR spectrum of PANI were located at 1571 and 1488  $\text{cm}^{-1}$ , respectively, and red-shifted to 1560 and 1481  $\text{cm}^{-1}$  in FT-IR spectrum of MCP-3, respectively, which indicated the higher conjugated extent of MCP-3 than that of PANI. It was also obvious that the peak intensity of the stretching vibration of aromatic ring at 1664  $\text{cm}^{-1}$  significantly increased in FT-IR spectrum of MCP-3 compared with that in FT-IR spectrum of PANI, which indicated an increase in the benzenoid content because of the copolymerization of aniline, PPDA and TPA [21]. Moreover, the C-H stretching vibrations of methylene located at 2850 and 2915  $\text{cm}^{-1}$  in FT-IR spectrum of

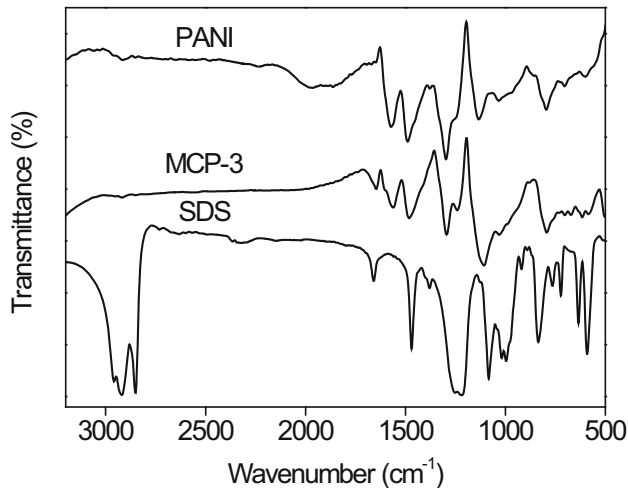


**Figure 1** FT-IR spectra of PANI, MCP-3 and SDS.

SDS were not observed in FT-IR spectrum of MCP-3, which demonstrated the complete removal of SDS from MCP-3.

UV-Vis absorption spectra of PANI and MCP dispersed well in DMF are presented in Fig. 2. The peaks at 300–330 nm and 550–650 nm were assigned to the  $\pi \rightarrow \pi^*$  benzenoid transition and  $\pi \rightarrow \pi^*$  quinonoid transition, respectively, and the latter peak indicated the emeraldine base forms of PANI and MCP [22]. When the intensity of absorption peak at 300–330 nm was normalized, it was obvious that the intensity of absorption peak at 550–650 nm became weak and then strong with the increase of the feeding molar ratio of SDS to aniline and MCP-3 showed the weakest intensity of absorption peak at 550–650 nm than other samples, which demonstrated that MCP-3

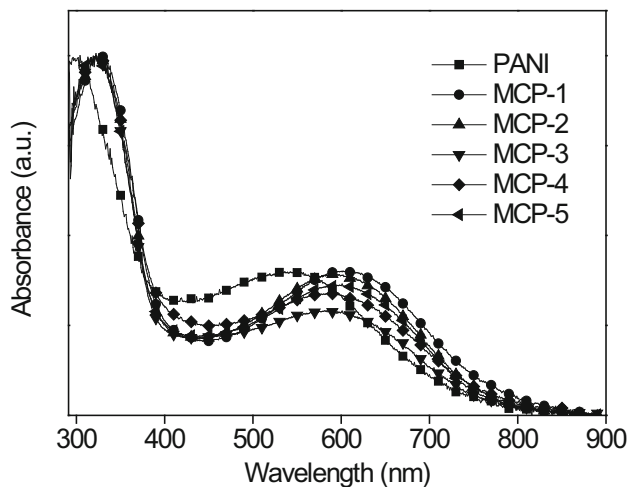


**Figure 2** UV-Vis absorption spectra of PANI and MCP.

had the highest doping level. Moreover, the energy required for the  $\pi \rightarrow \pi^*$  quinonoid transition of MCP was reduced due to their high conjugated extent, so that the absorption peak assigned to the  $\pi \rightarrow \pi^*$  quinonoid transition occurred red shift from 540 nm in UV-Vis absorption spectrum of PANI to 610 nm in UV-Vis absorption spectra of MCP.

### Morphology and formation mechanism

The SEM images of PANI and MCP are shown in Fig. 3, and the inset was the TEM image of MCP-3. In the SEM image of PANI, it was found that a large number of PANI blocks stacked together and many large spaces existed among the PANI blocks. In the SEM images of MCP, the sizes of PANI blocks and the spaces existing among the PANI blocks decreased, besides, some mesopores were observed in the PANI blocks and the number of mesopores increased with the increase of the feeding molar ratio of SDS to aniline. In addition, the mesoporous structure was proved by the TEM image of MCP-3.

The formation mechanism of MCP is illustrated in Fig. 4. Since the Krafft point of SDS was around 16 °C, SDS could form micelles at 25 °C, which would be used as template for the synthesis of MCP. Van Os et al. [23] reported that the critical micelle concentration (CMC) of SDS was 8.0 mmol/L in aqueous solution without any additives at 20 °C. At this concentration, the shape of micelle was assumed to be spherical, and the size of micelle and the aggregation number of SDS were approximately 6 nm in diameter and 62, respectively. When solubilize, salt, or any other additives were added, the aqueous solution of SDS became so complex that the shape, size and morphology of micelle could not be predicted without experimental investigation. The aggregation number of SDS at 0.18 mol/L in 0.1 mol/L NaCl aqueous solution was reported to be 92 at 25 °C, and the size of micelle was assumed to be around 15 nm in diameter [23]. A possible reason was that the electrostatic interaction of salt ion with sulfate ion of SDS could weaken the electrostatic repulsion among sulfate ions of SDS molecules and lead to an increase in the size of micelle.

Generally, the shape of micelle in a more complex solution could change from sphere to cylinder, hexagonal and lamellar structure successively with the increase of SDS concentration [24]. In this work, SDS concentration ranged from 0.05 to 0.5 mol/L, so



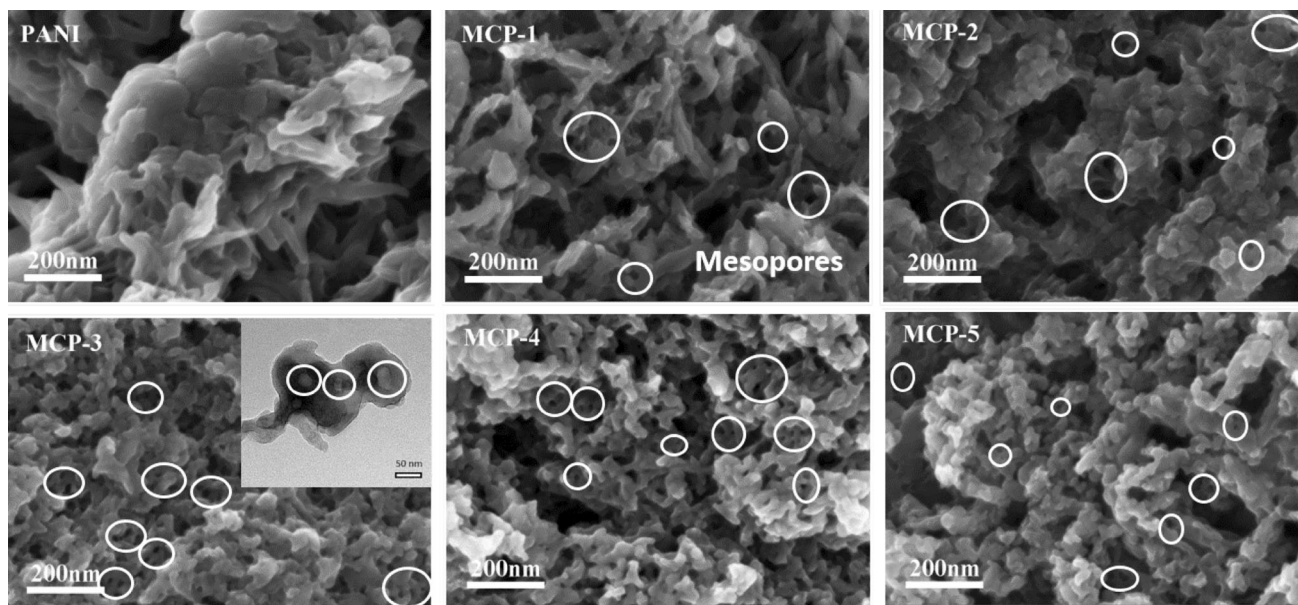


**Figure 3** SEM images of PANI and MCP, and the inset was the TEM image of MCP-3.

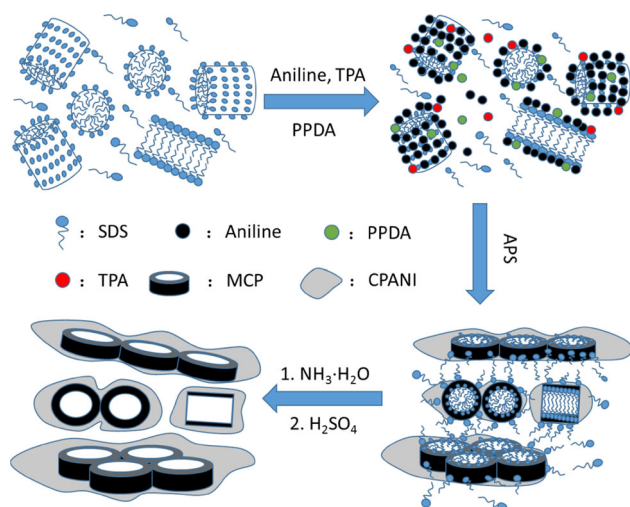


**Figure 4** Formation mechanism of MCP.

it could be considered reasonably that the shapes of SDS micelles were sphere and cylinder, and the content of cylindrical micelle increased with the increase in SDS concentration. During the process of chemical oxidation polymerization of aniline, aniline cations and PPDA cations were adsorbed on the surface of micelles by electrostatic interaction [25] and oxidized into phenylamino cationic radicals by APS, and then these phenylamino cationic radicals polymerized into linear poly(aniline-*p*-phenylenediamine) oligomers with two terminated amino groups on the surface of micelles that were used as templates. The poly(aniline-*p*-phenylenediamine)

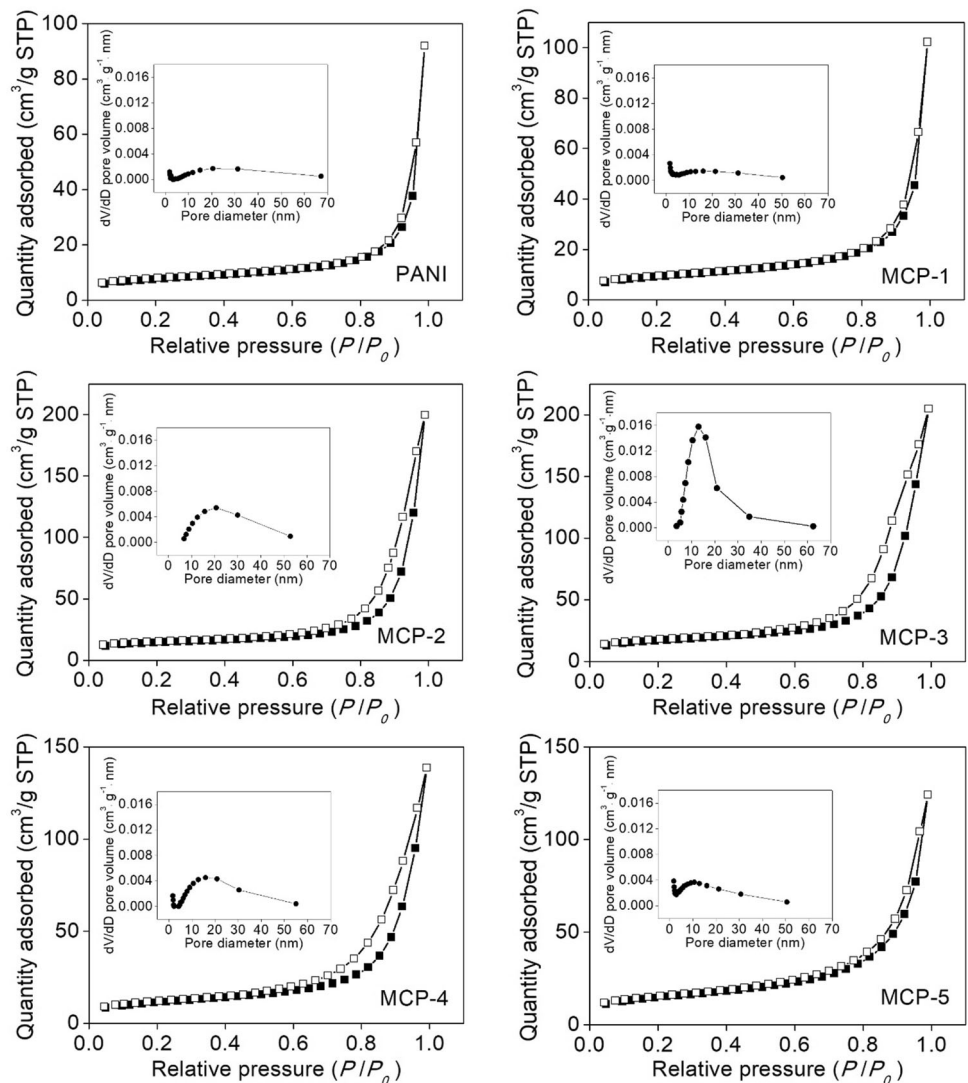
oligomers continued to react with TPA to form CPANI [26]. Because of the free SDS molecules, a small amount of CPANI could be stably dispersed in aqueous solution. When a large amount of CPANI formed, the stabilizing effect of SDS molecules weakened, and CPANI precipitated with the SDS molecules. After polymerization, the spherical and cylindrical micelles covered by CPANI and the SDS molecules attaching onto CPANI were removed by  $\text{NH}_3 \cdot \text{H}_2\text{O}$  to form MCP. Thus, the space left by the removal of the SDS molecules attached onto CPANI also made contribution to the specific surface area of MCP.

### BET analysis

It was found in Fig. 5 that the adsorption–desorption isotherm of PANI and MCP exhibited the obvious characteristic of Type IIb, a Type II isotherm with the H3 hysteresis, and the inset shows the corresponding pore size distribution of meso/macropores obtained by the Barrett–Joyner–Halenda (BJH) method. For PANI, the profile of pore size distribution was relatively flat, which indicated that the pore size distribution of PANI was irregular. By comparison with PANI, the pore diameter of MCP was mainly in the range of 5–35 nm, which certified that MCP was a sort of mesoporous materials.

The specific surface areas of PANI and MCP are listed in Table 1, which revealed that each total

**Figure 5** Adsorption–desorption isotherms of PANI and MCP, solid and open symbols were of adsorption and desorption branches, respectively, and the inset shows the corresponding pore size distribution obtained by BJH method.



specific surface area of MCP was much higher than that of PANI. The total specific surface area of MCP showed an increase with the increase in feeding molar ratio of SDS to aniline and achieved its maximum value of 59.2 cm<sup>2</sup>/g when the feeding molar ratio was 5:1, and the total specific surface area of MCP began to decrease with further increase in feeding molar ratio of SDS to aniline and attained a small value of 40.1 cm<sup>2</sup>/g when the feeding molar ratio was 10:1. The mesoporous structure and high specific surface area of MCP were favorable for ion transfer, and hence, MCP could promise excellent capacitance performance when it was used as electrode materials for redox supercapacitors.

**Table 1** Specific surface areas of PANI and MCP

Sample	Specific surface area (m <sup>2</sup> /g) <sup>a</sup>		
	$S_{\text{total}}$	$S_{\text{meso/macro}}$	$S_{\text{micro}}$
PANI	26.3	20.1	6.2
MCP-1	32.2	26.0	6.2
MCP-2	44.6	29.4	14.2
MCP-3	59.2	44.7	14.5
MCP-4	52.4	42.6	9.8
MCP-5	40.1	35.1	5.0

<sup>a</sup>Total surface area ( $S_{\text{total}}$ ) and meso/macropore surface area ( $S_{\text{meso/macro}}$ ) were obtained from an  $\alpha_{\text{SPE}}$ -plot and  $t$ -plot, respectively. Micropore surface area ( $S_{\text{micro}}$ ) was calculated by subtracting  $S_{\text{meso/macro}}$  from  $S_{\text{total}}$

## XRD measurement

Figure 6 shows the X-ray powder diffraction patterns of PANI and MCP. For PANI, the diffraction peaks at  $2\theta = 15.2^\circ$ ,  $20.6^\circ$  and  $25.3^\circ$  could be attributed to the (011), (020) and (200) crystal planes in its emeraldine salt form, respectively [27]. Although it was reported that PPDA had no effect on the crystallinity of PANI [28–30], the diffraction peaks at  $15.2^\circ$  and  $25.3^\circ$  of MCP decreased in relative intensity compared to that of PANI in this paper, which might be owing to that the copolymerization of poly(aniline-*p*-phenylenediamine) oligomer with TPA would hinder the ordered arrangement of PANI chain [31, 32], and reduce the orientation degree and the number of crystallites in the (011) and (200) crystal planes of MCP. Moreover, no visible diffraction peaks were observed in the range of  $5^\circ$ – $10^\circ$  in the XRD patterns of MCP, which suggested that the mesopores in MCP were arranged in disorder.

## TGA analysis

The thermal stabilities of PANI and MCP-3 were investigated by TGA analysis, and the TGA curves of PANI and MCP-3 are shown in Fig. 7. The initial weight losses of PANI and MCP-3 in the temperature range of  $30$ – $150^\circ\text{C}$  were caused by the evaporation of moisture. The weight losses of PANI and MCP-3 were related to the removal of sulfate anions in the range of temperature from  $200$  to  $360^\circ\text{C}$  [33], and MCP-3 showed a higher mass loss (16.36 wt%) than that of PANI (12.51 wt%) due to its higher doping

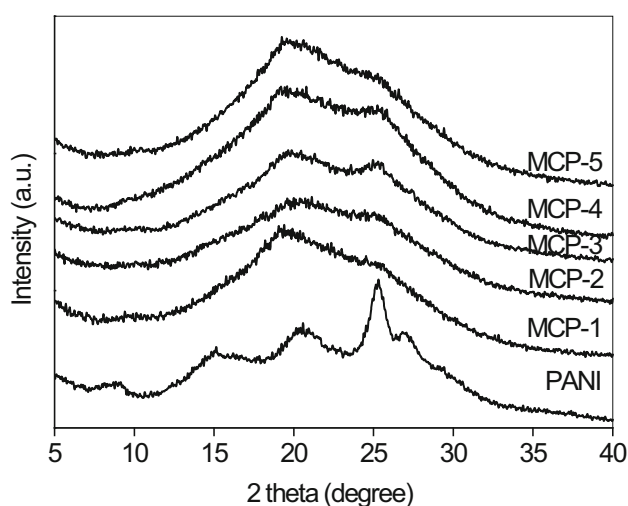


**Figure 6** XRD patterns of PANI and MCP.

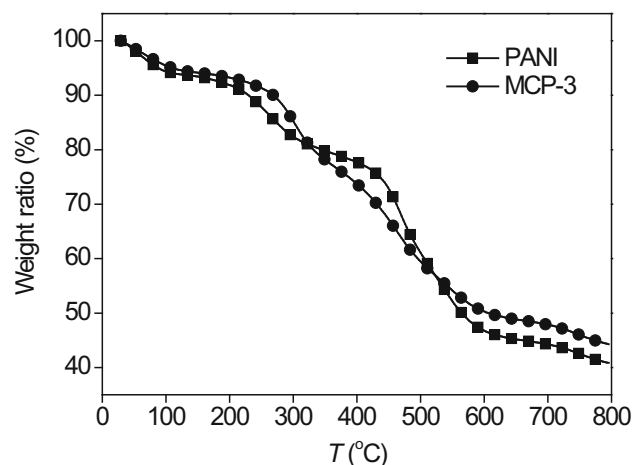


**Figure 7** TGA curves of PANI and MCP-3.

level, which was consistent with the results observed by spectral analysis. The weight losses in the temperature range of  $360$ – $660^\circ\text{C}$  corresponded to the decomposition of PANI and MCP-3 chains and the remained weights of MCP-3 and PANI were estimated to be 38.75 and 32.55 wt% of their initial weights, respectively. The relatively smaller weight loss of MCP-3 than that of PANI could be attributed to the hindering effect of crosslinking structure of MCP-3 on the decomposition of its chain.

## Conductivity

The conductivities of PANI and MCP are listed in Table 2. It was found that each MCP sample showed much higher conductivity than PANI. The conductivity of MCP showed an increase with the increase in feeding molar ratio of SDS to aniline and achieved its maximum value of  $24.1\text{ S/cm}$  when the feeding molar ratio was 5:1. The conductivity of MCP began to decrease with further increase in feeding molar ratio of SDS to aniline and attained a small value of  $14.9\text{ S/cm}$  when the feeding molar ratio was 10:1. It was obvious that the variation trend of conductivity of MCP was consistent with that of intensity of UV–Vis absorption peak at  $550$ – $650\text{ nm}$  with the increase in feeding molar ratio of SDS to aniline, which demonstrated that the increased conductivity of MCP was due to its high doping level and conjugated extent.

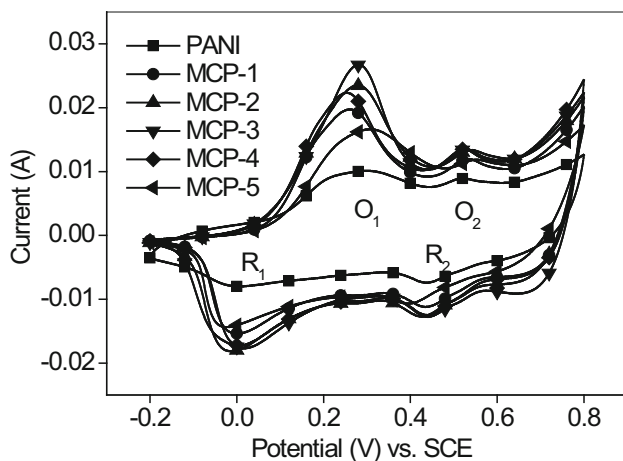
**Table 2** Conductivities of PANI and MCP

Sample	PANI	MCP-1	MCP-2	MCP-3	MCP-4	MCP-5
Conductivity (S/cm)	1.37	10.5	16.5	24.1	19.4	14.9

### Electrochemical test

Figure 8 displays the CV curves of PANI and MCP. It was found that both PANI and MCP showed the typical reduction peaks (peak  $R_1$  and  $R_2$ ) and oxidation peaks (peak  $O_1$  and  $O_2$ ) of PANI, which were attributed to the redox conversion of leucoemeraldine/emeraldine (peak  $O_1$  and  $R_1$ ) and emeraldine/parnigraniline (peak  $O_2$  and  $R_2$ ) [34]. It was also observed obviously that the area surrounded by CV curve of each MCP sample was larger than that of PANI, which foreshadowed a larger specific capacitance.

The GCD curves of PANI and MCP at a current density of 2 A/g are shown in Fig. 9a, and the corresponding specific capacitances are listed in Table 3. The almost symmetric GCD curves showed good capacitive behavior of PANI and MCP at large-scale current densities. It was observed clearly that the internal resistance (IR) of each MCP sample was smaller than that of PANI and MCP-3 had the smallest IR value, which signified that PS-3 possessed the lowest internal resistance. It is also found in Table 3 that the specific capacitance of PANI was 293 F/g and the specific capacitance of MCP increased firstly and then decreased with the increase in feeding molar ratio of SDS to aniline, and MCP showed the largest specific capacitance of 516 F/g when the feeding molar ratio of SDS to aniline was 5:1. The

**Figure 8** CV curves of PANI and MCP at a scan rate of 5 mV/s.

excellent specific capacitance of MCP could be attributed to their high conductivity and special mesoporous crosslinking structure with large specific surface area, which could promote the charge conduction and provide a large electrode–electrolyte interface area in favor of the participation of active material in the redox reaction. The plots of specific capacitance for PANI and MCP at various current densities are shown in Fig. 9b. It was clearly revealed that the decrease degree of specific capacitance of each MCP sample was lower than that of PANI with the increase in current density, which demonstrated that the rate capability of MCP was much better than that of PANI.

In order to further study the effect of crosslinked structure on the electrochemical cycling stability of MCP, PANI and MCP-3 were performed by CV test for 2000 cycles at a scan rate of 100 mV/s in the range of  $-0.2$  to  $0.8$  V, respectively, and the corresponding specific capacitance retentions are shown in Fig. 10. The SEM images of MCP-3 after CV test for 1, 1000 and 2000 cycles are also shown in Fig. 10. It was found that MCP-3 presented good electrochemical cycling stability and retained 73.2% of its initial specific capacitance after 2000 cycles, while PANI kept only 48.2% of its initial specific capacitance after 2000 cycles. As shown in Fig. 10, although the mesoporous structure of MCP-3 collapsed partly after a long charge–discharge process, a small number mesopores could still be observed clearly because of its special crosslinking structure, which was favorable to the improvement in electrochemical cycling stability of MCP-3.

EIS measurements of PANI and MCP-3 were presented in terms of Nyquist plots as shown in Fig. 11. The Nyquist plots of PANI and MCP-3 were all consisted of an incomplete semicircle at the high frequency region and a straight line at the low frequency region. The charge transfer resistance ( $R_{ct}$ ) was a characteristic quantity for the charge transfer step of an electrode reaction that was calculated by the diameter of semicircle [35, 36]. The  $R_{ct}$  value of PANI and MCP-3 was 0.227 and 0.121  $\Omega$ , respectively. The smaller  $R_{ct}$  value of MCP-3 than that of PANI could be explained by its high conductivity



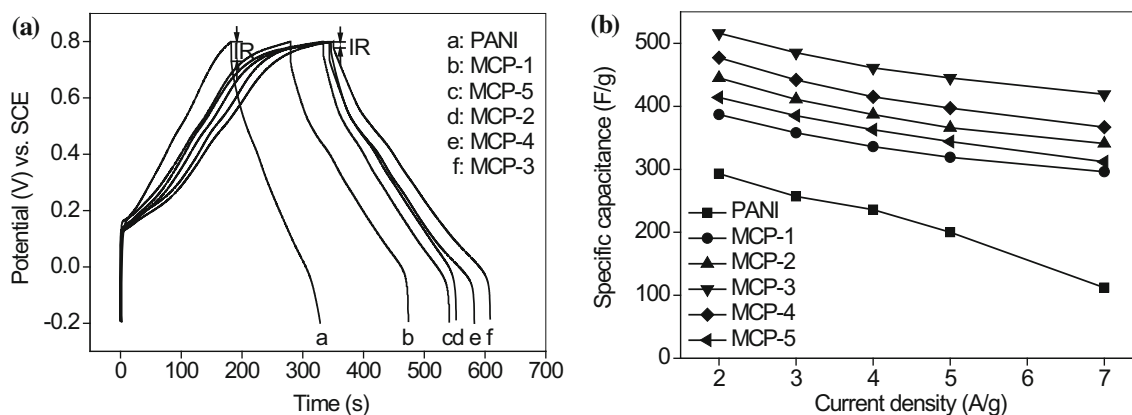


**Figure 9** GCD curves of PANI and MCP at a current density of 2 A/g (a) and plots of specific capacitance for PANI and MCP at various current densities (b).

**Table 3** Specific capacitances for PANI and MCP at a current density of 2 A/g

Sample	PANI	MCP-1	MCP-2	MCP-3	MCP-4	MCP-5
Specific capacitance (F/g)	293	387	445	516	477	414

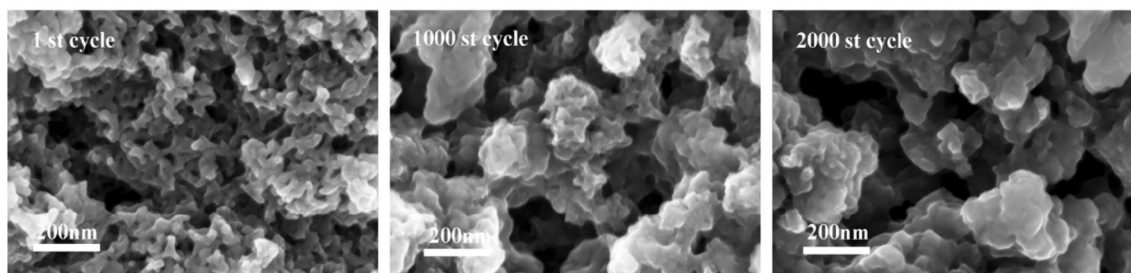
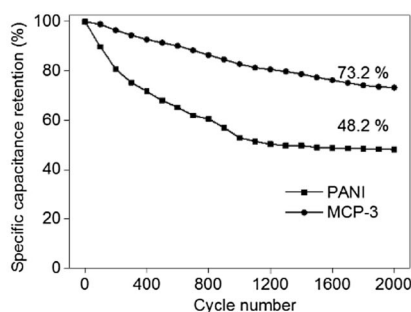


**Figure 10** Electrochemical cycling stabilities of PANI and MCP-3 and SEM images of MCP-3 after CV test for 1, 1000 and 2000 cycles, respectively.

and disordered mesoporous structure, which would shorten the diffusion path of electrolyte ion and facilitate the charge to transfer into the interior of MCP-3.

### Conclusions

MCP was prepared successfully via chemical oxidative polymerization by copolymerizing aniline and PPDA with TPA as crosslinker, using SDS as a soft template and APS as an oxidant. SEM observation revealed the existence of some mesopores in MCP and the importance of SDS micelles during the process of forming mesopores. BET analysis and XRD

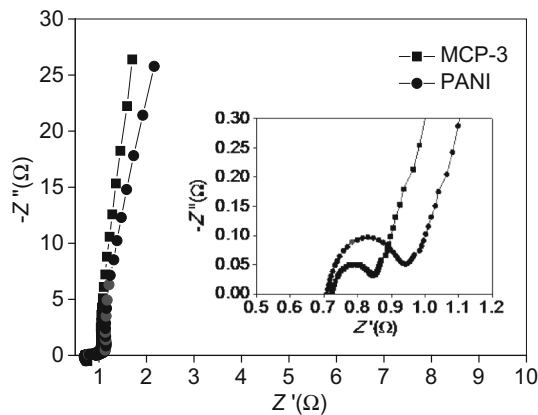


**Figure 11** Nyquist plots of PANI and MCP-3.

measurement further proved the existence of disordered mesopores with diameters of 5–35 nm and the largest specific surface area of 59.2 m<sup>2</sup>/g. Spectral studies and TGA analysis provided the evidences that MCP had the high doping level and special crosslinking structure. In addition, MCP showed the highest conductivity of 24.1 S/cm, largest specific capacitance of 516 F/g at 2 A/g and good specific capacitance retention of 73.2% after 2000 cycles when the feeding molar ratio of SDS to aniline was 5:1, which were ascribed to the synergistic effects of high doping level, special mesoporous crosslinking structure and large specific surface area. The reasonable large value of specific capacitance with good electrochemical cycling stability of MCP certified its efficiency as electrode material for supercapacitors.

## Acknowledgements

This work was supported by the National Natural Science Foundation of China (Grant No. 61205182).

## References

- [1] Kotz R, Carlen M (2000) Principles and applications of electrochemical capacitors. *Electrochim Acta* 45:2483–2498
- [2] Conway BE (1999) *Electrochemical supercapacitors: scientific fundamentals and technological applications*. Springer, New York
- [3] Pandolfo AG, Hollenkamp AF (2006) Carbon properties and their role in supercapacitors. *J Power Sources* 157:11–27
- [4] Chmiola J, Yushin G, Gogoti Y, Portet C, Simon P, Taberna PL (2006) Anomalous increase in carbon capacitance at pore sizes less than 1 nanometer. *Science* 313:1760–1763
- [5] Yamada H, Tagawa K, Komatsu M, Moriguchi I, Kudo T (2007) High power battery electrodes using nanoporous V<sub>2</sub>O<sub>5</sub>/carbon composites. *J Phys Chem C* 111:8397–8402
- [6] Fan LZ, Maier J (2006) High-performance polypyrrole electrode materials for redox supercapacitors. *Electrochem Commun* 8:937–940
- [7] Barbieri O, Hahn M, Foelske A, Kotz R (2006) Effect of electronic resistance and water content on the performance of RuO<sub>2</sub> for supercapacitors. *J Electrochem Soc* 153:A2049–A2054
- [8] Zhang H, Cao GP, Yang YS (2009) Carbon nanotube arrays and their composites for electrochemical capacitors and lithium-ion batteries. *Energy Environ Sci* 2:932–943
- [9] Li XW, Zhang H, Wang GC, Jiang ZH (2010) A novel electrode material based on a highly homogeneous polyaniline/titanium oxide hybrid for high-rate electrochemical capacitors. *J Mater Chem* 20:10598–10601
- [10] Park JH, Park OO, Shin KH, Jin CS, Kim JH (2002) An electrochemical capacitor based on a Ni(OH)<sub>2</sub>/activated carbon composite electrode. *Electrochem Solid St* 5:H7–H10
- [11] Kovalenko I, Bucknall DG, Yushin G (2010) Detonation nanodiamond and onion-like-carbon-embedded polyaniline for supercapacitors. *Adv Funct Mater* 20:3979–3986
- [12] Fan LZ, Hu YS, Maier J, Adelhelm P, Smarsly B, Antonietti M (2007) High electroactivity of polyaniline in supercapacitors by using a hierarchically porous carbon monolith as a support. *Adv Funct Mater* 17:3083–3087
- [13] Wang X, Deng J, Duan X, Liu D, Guo J, Liu P (2014) Crosslinked polyaniline nanorods with improved electrochemical performance as electrode material for supercapacitors. *J Mater Chem A* 2:12323–12329
- [14] Pan L, Qiu H, Dou C, Li Y, Pu L, Xu JB, Shi Y (2010) Conducting polymer nanostructures: template synthesis and applications in energy storage. *Int J Mol Sci* 11:2636
- [15] Tian H, Zhu SY, Xu FG, Mao WT, Wei H, Mai YY, Feng XL (2017) Growth of 2D mesoporous polyaniline with controlled pore structures on ultrathin MoS<sub>2</sub> nanosheets by block copolymer self-assembly in solution. *ACS Appl Mater Interfaces* 9:43975–43982
- [16] Wang N, Tian H, Zhu SY, Yan DY, Mai YY (2018) Two-dimensional nitrogen-doped mesoporous carbon/graphene nanocomposites from the self-assembly of block copolymer micelles in solution. *Chin J Polym Sci* 36:266–272
- [17] Zhou CQ, Han JV, Guo R (2009) Polyaniline fan-like architectures of rectangular sub-microtubes synthesized in dilute inorganic acid solution. *Die Unterrichtspraxis/teaching German* 30:182
- [18] Zhou CQ, Han J, Guo R (2009) Synthesis of polyaniline hierarchical structures in a dilute SDS/HCl solution:

- nanostructure-covered rectangular tubes. *Macromolecules* 42:1252–1257
- [19] Zhou CQ, Han J, Guo R (2008) Dilute anionic surfactant solution route to polyaniline rectangular sub-microtubes as a novel nanostructure. *J Phys Chem B* 112:5014–5019
- [20] Xin GX, Wang YH, Jia SP, Tian PF, Zhou SY, Zang JB (2017) Synthesis of nitrogen-doped mesoporous carbon from polyaniline with an F127 template for high-performance supercapacitors. *Appl Surf Sci* 422:654–660
- [21] Yang YY, Chen SZ, Xu L (2011) Enhanced conductivity of polyaniline by conjugated crosslinking. *Macromol Rapid Comm* 32:593
- [22] Izumi CMS, Ferreira AMDC, Constantino VRL, Temperini MLA (2007) Studies on the interaction of emeraldine base polyaniline with Cu(II), Fe(III), and Zn(II) ions in solutions and films. *Macromolecules* 40:3204
- [23] Van Os NM, Haak JR, Rupert LA (1993) Physico-chemical properties of selected anionic, cationic and nonionic surfactants. Elsevier, Amsterdam
- [24] Oh SG, Shah DO (1993) The effect of micellar lifetime on the rate of solubilization and detergency in sodium dodecyl sulfate solutions. *J Am Oil Chem Soc* 70:673–678
- [25] Kuramoto N, Tomita A (1997) Aqueous polyaniline suspensions: chemical oxidative polymerization of dodecylbenzene-sulfonic acid aniline salt. *Polymer* 38:3055–3058
- [26] Lange U, Roznyatovskaya NV, Mirsky VM (2008) Conducting polymers in chemical sensors and arrays. *Anal Chim Acta* 614:1–26
- [27] Chaudhari HK, Kelkar DS (1997) Investigation of structure and electrical conductivity in doped polyaniline. *Polym Int* 42:380–384
- [28] Shenashen MA, Ayad MM, Salahuddin N, Youssif MA (2010) Usage of quartz crystal microbalance technique to study the polyaniline films formation in the presence of *p*-phenylenediamine. *React Funct Polym* 70:843–848
- [29] Niu HJ, Luo PH, Zhang ML, Zhang L, Hao LN, Luo J, Bai XD, Wang W (2009) Multifunctional, photochromic, acid-ichromic, electrochromic molecular switch: novel aromatic poly(azomethine)s containing triphenylamine group. *Eur Polym J* 45:3058–3071
- [30] Liu P, Zhang P, Cao DL, Gan LH, Li YF (2013) New side groups-tuned triphenylamine-based chromophores: synthesis, morphology, photophysical properties and electronic structures. *J Mol Struct* 1050:151–158
- [31] Jozefowicz ME, Epstein AJ, Pouget JP, Masters JG, Ray A, MacDiarmid AG (1991) X-ray structure of the polyaniline derivative poly(*o*-toluidine): the structural origin of charge localization. *Macromolecules* 24:5863–5866
- [32] Bhadra S, Khastgir D (2008) Determination of crystal structure of polyaniline and substituted polyanilines through powder X-ray diffraction analysis. *Polym Test* 27:851–857
- [33] Gemeay AH, El-Sharkawy RG, Mansour IA, Zaki AB (2007) Preparation and characterization of polyaniline/manganese dioxide composites and their catalytic activity. *J Colloid Interf Sci* 308:2575–2583
- [34] Wang YG, Li HQ, Xia YY (2006) Ordered whiskerlike polyaniline grown on the surface of mesoporous carbon and its electrochemical capacitance performance. *Adv Mater* 18:2619–2623
- [35] Rajeswari J, Kishore PS, Viswanathan B, Varadarajan TK (2009) One-dimensional MoO<sub>2</sub> nanorods for supercapacitor applications. *Electrochem Commun* 11:572–575
- [36] Li X, Rong J, Wei B (2010) Electrochemical behavior of single-walled carbon nanotube supercapacitors under compressive stress. *ACS Nano* 4:6039–6049